Stereophotography of rain drops and compound poisson - cascade processes

S. Lovejoy[1], D. Schertzer[2]

[1]Department of Physics, McGill University, 3600 University st., Montreal, Que., Canada

[2]CEREVE, Ecole Nationale des Ponts et Chaussées, 6-8, avenue Blaise Pascal, Cité Descartes, 77455 MARNE-LA-VALLEE Cedex, France

Abstract:

Precipitation and clouds are fundamentally point-like but when averaged over larger enough scales are usually considered to be continuous and are mathematically modeled using fields (or densities of measures). Until recently when it has been essential to have a particle description, the latter have been modeled using uniform Poisson processes in which the number density of particles is considered uniform in space and/or time. Since empirical drop distributions (typically measured with disdrometers) are never spatially or temporally homogeneous, attempts have been made to model the heterogeneity using classical compound Poisson processes in which heterogeneity over narrow ranges of scales "control" the Poisson process.

While the disdrometer based experiments have increasingly recognized the importance of drop heterogeneity, there has been a growing consensus – at least over the smaller scales – that atmospheric turbulence can be accurately modeled by cascade processes in which energy and other conservative fluxes are concentrated into a hierarchy sparse fractal sets, (more precisely, multifractal measures) in which the heterogeneity occurs over huge ranges of space-time scales in a power law manner. Since the turbulent wind and the drops are strongly coupled, it is natural to suppose that the drop heterogeneity also occurs over wide ranges, and that the latter is largely "controlled" by the turbulence. Recently [*Lovejoy, et al.*, 2003], [*Lilley, et al.*, 2005] the connection between the drop statistics and (Corrsin-Obukov) turbulence has been directly made thanks to the use of stereophotography of rain drops in $10m^3$ volumes (the "HYDROP" experiment [*Desaulniers-Soucy., et al.*, 2001]).

In this paper, we show how the turbulence and particle processes can be combined in a nonclassical compound Poisson-cascade process and we verify the result on the HYDROP data. The key is the liquid water density ρ variance flux (χ) which - following the HYDROP observations and Corrsin-Obukhov passive scalar theory – is conserved from scale to scale (it is the basic multifractal field). The link to the particle description is via the particle number density (n); we show how this can be determined from χ and the turbulent energy flux ε; we theoretically predict a (classical) $k^{-5/3}$ spectrum for ρ and a new k^{-2} spectrum for n which we confirm is close to observations.

In order to perform simulations respecting these turbulence constraints we start with cascade models of χ and ε cut-off by viscosity at the dissipation scale (roughly 1cm). From these fluxes we determine ρ and n by fractional integration. At scales below 10cm or so, there is typically only one drop in the corresponding sphere; we interpret n as the number density of a (compound) Poisson process and randomly determine the positions of the ith particle: $\underline{x}_i$. The masses m_i, are determined from a unit exponential (Marshall-Palmer) random variable u_i: $m_i = u_i \rho(\underline{x}_i)/n(\underline{x}_i)$. The resulting measure (m_i, $\underline{x}_i$) has the observed energy spectrum, the observed multifractal statistics (including the transition from particle scales to field scales) it also has realistic probability (fat tailed, power law) distributions for total mass in a large sphere M. In this case, it predicts a power law with exponent $q_D = 3$ (this is an exact result coming

---

[1] Corresponding author: Department of Physics, McGill University, 3600 University st., Montreal, QC, Canada, H3A 2T8,

e-mail: lovejoy@physics.mcgill.ca

from theory and dimensional analysis). We show both on numerical simulations and on the HYDROP data that this prediction is accurately obeyed. In addition, it potentially explains several reports that $q_D \approx 3$ for the rain rate. Since it incorporates (in a highly inhomogeneous framework) the Marshall-Palmer exponential drop distribution as well as a Poisson particle process, it bridges the gap between classical and turbulence approaches.

Numerical simulations spanning the range 1cm to 1000km can be readily produced. These simulations can be used for simulating radar reflectivity factors, effective radar reflectivity factors; extensions of the model can be used to simulate rain rates and rain gauges. These models can thus potentially solve various precipitation observer problems.

1. Introduction

Rain is a highly turbulent process yet there is widening gap between turbulence and precipitation research. On the one hand turbulence is increasingly viewed as a highly intermittent, highly heterogeneous process with turbulent energy, passive scalar variance and other fluxes concentrated into a hierarchy of increasingly sparse fractal sets; over wide ranges, the fields are multifractal (see e.g. [*Anselmet*, 2001] for a recent review). Furthermore, advances in high powered lidars have produced turbulent atmospheric data sets of unparalleled space-time resolution. Analysis of such data from aerosols have shown that if classical Corrsin-Obukhov theory of passive scalar turbulence is given anisotropic extensions to account for atmospheric stratification and multifractal extensions to account for intermittency, that these rejuvenated classical theories account remarkably well for passive pollutants ([*Lilley, et al.*, 2004]). In contrast, applications of turbulence theory either to interpreting radar echoes, or to disdrometer experiments almost invariably assume that the turbulence is uniform resulting in homogeneous Poisson rain statistics (e.g. [*Marshall and Hitschfeld*, 1953], [*Wallace*, 1953]), or that it is only weakly heterogeneous and can be modeled by ad hoc compound Poisson processes (e.g. [*Uijlenhoet, et al.*, 1999], [*Jameson and Kostinski*, 1999]).

At a theoretical level, combining turbulence theory with rain drop physics poses two related difficulties. One the one hand rain is particulate and is strongly coupled to the multifractal wind field so it is not continuous and its classical treatment as a mathematical space-time field (e.g. that $R(\underline{x},t)$ is well defined without explicit reference to its scale/resolution) is not obvious ([*Lovejoy, et al.*, 2003]). One the other hand, it does not obviously fit into the classical turbulence framework of passive scalars: rain simultaneously modifies the wind field while moving with speeds from different than that of the ambient air. So far, attempts to attack the full interaction at its most fundamental level by taking these two aspects into explicitly into account (e.g. [*Falkovitch and Pumir*, 2004], [*Falkovitch, et al.*, 2006]), have made limited progress. At a more phenomenological level, there has been more progress following the proposal ([*Schertzer and Lovejoy*, 1987]) that even if rain is not a passive scalar that it nevertheless has an associated scale-by-scale conserved turbulent flux leading to a coupled turbulence/rain cascade model and predicting multifractal rain statistics over wide ranges of scale. The predictions that rain should have anisotropic (especially stratified) multifractal statistics although based essentially on the use of scaling symmetry arguments has been quite fruitful (see e.g. the early review [*Lovejoy and Schertzer*, 1995]). However these empirical studies have been at scales larger than drop scales and outstanding problems include the characterization of low rain rate events and the

identification of the conserved (cascaded) flux itself. In other words, the connection with turbulence has remained implicit rather than explicit.

In order to bridge the gap between the drop physics and turbulence, data spanning the drop and turbulence scales were needed. Starting in the 1980's, various attempts have been made including experiments with chemically coated blotting paper ([*Lovejoy and Schertzer*, 1990]) and lasers, ([*Lovejoy and Schertzer*, 1991]). The most satisfactory of these was the HYDROP experiment ([*Desaulniers-Soucy., et al.*, 2001]) which involved stereophotography of rain drops in $\approx 10\text{m}^3$ volumes typically capturing the position and size of 5,000 -20,000 drops (nominal rain rates were between 2 and 10mm/hr; see fig. 1 for an example, and table 1 for information about HYDROP). Analyzes to date ([*Lovejoy, et al.*, 2003], [*Lilley, et al.*, 2005]) have shown that at scales larger than a characteristic scale determined by both the turbulence intensity and the drop size distribution (but typically around 20-30 cm see e.g. fig. 1a, b) that the liquid water content (LWC) and other statistics cluster in a scaling manner as predicted by cascade theories. While these results suggested that rain is strongly coupled to the turbulent wind field at scales larger than 20-30cm (potentially explaining the multifractal properties of rain observed at much larger scales), the analyses did not find an explicit connection with standard turbulence theory.

In this paper, we perform the first spectral analyses on the HYDROP data demonstrating quantitatively the connection with passive scalar advection. We then go on to propose a phenomenological turbulence - drop coalescence equation which we use as the basis for a compound multifractal process model of rain. The resulting model is based in turbulence theory yet generates realistic drop size distributions (including nonclassical extreme tails) and can be readily extended to account for spatial anisotropy (in particular, vertical stratification) and is very close to the HYDROP and other scaling analyses. It can be used for modeling radar measurements of rain from drop scales on up. Quite realistic (visually, statistically) radiative transfer and other simulations can be made, including for the low-zero rain rate regions.

2. The connection between drops and turbulence

2.1 Recap of the classical turbulence laws

In order to make a connection between the drop processes and turbulence, we recall the equations and phenomenology of passive scalar advection:

$$\frac{\partial \underline{v}}{\partial t} + \underline{v} \cdot \nabla \underline{v} = -\frac{1}{\rho_f} \nabla p + \nu \nabla^2 \underline{v} \qquad (1)$$

$$\nabla \cdot \underline{v} = 0 \qquad (2)$$

$$\frac{D\rho}{Dt} = \kappa \nabla^2 \rho; \quad \frac{D}{Dt} = \frac{\partial}{\partial t} + \underline{v} \cdot \nabla \qquad (3)$$

Eqs. 1, 2 are the standard fluid equations for the wind ($\underline{v}$, eq. 1), with incompressible continuity for the fluid density (ρ_f, eq. 2) and for passive scalar concentration (ρ, eq. 3). ν, κ are respectively the molecular viscosity and molecular diffusivity of the passive scalar, p is the pressure. In eq. 1 we have neglected the effect of gravity (this leads to a nontrivial scaling stratification discussed see e.g. [*Lilley, et al.*, 2004]; for simplicity here we assume isotropy in three dimensional space).

The standard Kolmogorov and Corrsin-Obukhov laws are obtained by noting that the nonlinear terms in the above conserve the fluxes:

$$\varepsilon = \frac{\partial v^2}{\partial t}; \quad \chi = \frac{\partial \rho^2}{\partial t} \qquad (4)$$

This follows by multiplying the equations by v, ρ respectively and using the incompressible continuity equation for $\underline{v}$ followed by standard manipulations.

One can also show that in fourier space the passive scalar variance flux χ and energy flux ε are indeed fluxes from large scales to small: according to the equations these fluxes are only dissipated at molecular scales. In addition, between an outer injection scale and the dissipation scale, there is no characteristic scale, hence at any intermediate scale l one expects:

$$\varepsilon_l \approx \frac{v_l^2}{\tau_l}; \quad \chi_l \approx \frac{\rho_l^2}{\tau_l} \qquad (5)$$

where v_l is the typical shear across an l sized eddy, and ρ_l is the corresponding typical gradient of passive scalar; the τ_l's are the corresponding transfer times (the "eddy turnover time" in turbulence jargon). In both cases the time scale is determined by the only relevant velocity and the length scale:

$$\tau_l = \frac{l}{v_l} \qquad (6)$$

This leads to:

$$\varepsilon_l \approx \frac{v_l^3}{l}; \quad \chi_l \approx \frac{\rho_l^2 v_l}{l} \qquad (7)$$

These equations lead directly to the classical Kolmogorov and Corrsin Obukhov laws:

$$v_l = \varepsilon_l^{1/3} l^{1/3} \qquad (8)$$

$$\rho_l = \chi_l^{1/2} \varepsilon_l^{-1/6} l^{1/3} \qquad (9)$$

laws. Finally, we might add that by invoking a third property of the equations – that they are "local" in fourier space, i.e. interactions are strongest between neighbouring scales, we obtain the standard cacade phenomenology, the basis of cascade models. In the 1980's it was discovered that such cascades generically yielded multifractal fluxes, hence accounting for turbulent intermittency.

2.2 The turbulence drop coalescence equation

Our aim is to find an equation analogous to eq. 3 but for rain liquid water concentration and which can account for both coalescence of drops and their decoupling from the ambient wind field due to drop inertia and gravity.

We first note that (ignoring condensation) the usual coalescence (Smolukowski) equation used for example in cloud and rain modeling [*Srivastava and Passarelli*, 1980] can be written:

$$\frac{\partial N}{\partial t} = \varphi \langle N|H|N \qquad (10)$$

where $N = N(M, \underline{x}, t)$ is the drop mass distribution function i.e. the number of drops with mass between M and $M+dM$ per unit volume of space at location $\underline{x}$, time t. The right hand side term is (in compact notation, see [*Lovejoy, et al.*, 2004]), the drop coalescence term where $\varphi(\underline{x}, t)$ is the coalescence rate and $\langle N|H|N$ is the coalescence operator:

$$\langle N|H|N = \frac{1}{2} \int_0^M H(M - M', M) N(M - M', \underline{x}, t) N(M', \underline{x}, t) dM'$$

$$-N(M, \underline{x}, t) \int_0^\infty H(M', M) N(M', \underline{x}, t) dM'$$

$$(11)$$

The full coalescence kernel $\mathbf{H}$ has been factorized $\mathbf{H}(M', M, \underline{x}, t) = \varphi(\underline{x}, t) H(M', M)$ so that the drop-drop collision mechanism is time-space independent: $H(M', M)$, space-time variations are accounted for by φ.

Motivated by the preceeding, we propose the following turbulent-drop coalescence equation:

$$\frac{\partial N}{\partial t} + \underline{v} \cdot \nabla N = \kappa_d(N) + \varphi(\underline{x}, t) \langle N|H|N \quad (12)$$

where we have used the advective derivative (D/Dt, eq. 3) instead of $\partial/\partial t$ and added a new phenomenological drop diffusivity term with a dissipation function $\kappa_d(N)$ which is only important at the small scales. We shall

see below that there is a natural averaging scale where the wind/drop decoupling occurs (in the data analyzed, at around 30cm), this dissipation term accounts for the deviation of drop velocities from the wind velocity $\underline{v}$ due to the fall speeds. This could be regarded as our "parametrization" assumption since in a single term we include all the non wind-advected drop motions. At this stage, this term is unimportant, we do not specify it explicitly; recall that for passive scalars, the dissipation is via molecular diffusion so that $\kappa_d(\mathsf{N}) = \kappa \nabla^2 \mathsf{N}$. In the form given it assures that the drop scale processes dominate at small scales where gradients in N are important, it also assures that the usual passive scalar advection equation is obtained at larger scales. With the exception of the dissipation term, eq. 12 is the same as that invoked in [*Falkovitch, et al.*, 2006] (although only the non turbulent $\underline{v}=0$ case was considered).

We now consider the first two moments of the turbulence-drop coalescence equation; the number density (n) and drop mass density (ρ):

$$n(\underline{x},t) = \int_0^\infty N(M,\underline{x},t)dM; \quad \rho(\underline{x},t) = \int_0^\infty N(M,\underline{x},t)MdM$$
(13)

We now multiply eq. 12 by dM and MdM respectively and integrate with respect to M. The results are:

$$\frac{\partial n(\underline{x},t)}{\partial t} + \underline{v} \cdot \nabla n = \kappa_d \nabla^2 n - \varphi(\underline{x},t)\langle \mathsf{N}|\mathsf{H}|\mathsf{N}\rangle$$
(14)

$$\frac{\partial \rho(\underline{x},t)}{\partial t} + \underline{v} \cdot \nabla \rho = \kappa_d \nabla^2 \rho$$
(15)

where

$$\langle \mathsf{N}|\mathsf{H}|\mathsf{N}\rangle = \int_0^\infty \langle \mathsf{N}|\mathsf{H}|\mathsf{N}dM$$
(16)

and where we have used the fact that the coalescence operator conserves drop mass:

$$\langle \mathsf{N}|\mathsf{H}|\mathsf{N}M\rangle = \int_0^\infty \langle \mathsf{N}|\mathsf{H}|\mathsf{N}MdM = 0$$
(17)

but not number so that for the ρ equation (15), coalescence is not directly relevant whereas it is relevant for the n equation (14).

By comparing equations 14, 15, we can see that the right hand side (dissipation terms) are quite different, so that it is quite possible that there in addition to χ (eq. 4), there is a new conserved flux ψ:

$$\psi = \frac{\partial n^2}{\partial t}$$
(18)

As in the above, we argue that in the scaling regime;

$$\psi_l \approx \frac{n_l^2}{\tau_{l,R}}$$
(19)

The key point here is that due to the importance of coalescence for n (but not ρ), that the time scale for the transfer is determined by rain drop scale processes, denoted $\tau_{l,R}$ which is not the same as the turbulent time scale ("eddy turn over time") $\tau_l = l/v_l$ relevant for ρ and hence χ. The time scale for the number variance flux ψ is determined by the coalescence processes and can be estimated from the particle fall speeds $v_{l,R}$ as:

$$\tau_{l,R} \approx \frac{l}{v_{l,R}}$$
(20)

where $v_{l,R}$ is a typical drop fall speed with respect to the local wind. Combining eq. 20, 18 we obtain:

$$n_l = v_{l,R}^{-1/2} \psi_l^{1/2} l^{1/2}$$
(21)

However, the fluxes χ, ψ are closely linked since they are both determined by different moments of N, indeed, since χ is quadratic in N, we expect at least for large enough averaging volumes:

$$\chi_l = \left(\overline{M^2}\right)_l \psi_l$$
(22)

where l is a spatial scale and:

$$\left(\overline{M^2}\right)_l = \frac{1}{vol(B_l)} \int_{B_l} M^2 P(M,\underline{x},t)dMd\underline{x}$$
(23)

where B_l is a "ball" (e.g. sphere) of scale l of volume $vol(B_l)$ and $P(M,\underline{x},t)$ is the probability density of particles with mass between M and $M+dM$:

$$P(M,\underline{x},t) = \frac{\mathsf{N}(M,\underline{x},t)}{n(\underline{x},t)} \qquad (24)$$

the mean mass is averaged over the drop probability distribution. Here and below, drop averaging is denoted by an overbar, and ensemble averaging over turbulent statistics (see below), by "<.>".

From eq. 21 and 22, we obtain the fundamental prediction of the turbulence-drop coalescence equation:

$$n_l = A_l \chi_l^{1/2} l^{1/2}; \quad A_l = \left(\left(\overline{M^2} \right)_l v_{l,R} \right)^{-1/2} \approx \left(\overline{M^2 v_R} \right)_l^{-1/2}$$
$$(25)$$

where:

$$\left(\overline{M^2 v_R} \right)_l = \frac{1}{vol(B_l)} \int_{B_l} M^2 v_R(M,\underline{x},t) P(M,\underline{x},t) dM d\underline{x} \qquad (26)$$

$v_R(M)$ is the characteristic (nonturbulent) fall speed of a drop of mass M. Physically this is plausible since v_R is the result of the decoupling of drops from the turbulence; this will be a kind of random walk with an overall drift imposed by gravity.

Eq. 26 is the key result of this section, in fourier space (ignoring multifractal intermittency corrections), this implies $E_n(k) \approx k^{-2}$ whereas for ρ, we have the classical Corrsin-Obukhov result: $E_\rho(k) \approx k^{-5/3}$. We shall see that the number density, combined with the mass density and assuming the scaling laws for v, ρ, n, all with assumptions about the statistics of the fluxes χ, ε, implicitly determine the drop size distributions.

3.   Empirical test of the number size distribution:

3.1 Discussion:

The key predictions of the turbulence –drop coalescence equation is that at least at large enough scales, the liquid water density follows the Corrsin-Obukhov ($l^{1/3}$) law, while the corresponding number density follows the new $l^{1/2}$ law (eq. 25). We thus seek to test both predictions using the HYDROP data.

Event ID	Date and time	Number of realizations	Volume of ROI (m³)	Number of rain-drops	Atmospheric conditions	Wind speed at 300 m (m s⁻¹)	Rain rate (mm h⁻¹)
f142	November 8th 1996, 7 p.m.	3	8.1	36422/3	Reflectivity bright band at 4 km: melting snow. Rain shower	2.5	2—4
f145	November 8th 1996, 8:30 p.m.	3	8.02	23708/3	Reflectivity bright band: melting snow. Rain shower	22.5	1.4—2.2
f207	July 14th 1997, 12:30 a.m.	7	7.87	59223/7	Convective. Heavy rain.	27.5	6—10
f229	November 1st 1997, 9:45 p.m.	2	7.13	30559/2	Reflectivity bright band at 4 km: melting snow. Embedded convection	17.5	2—4
f295	September 27th 1998, 2:50 a.m.	3	8.04	40100/3	Storm with light precipitation	10	1.4—2.2

Table 3   The atmospheric conditions were estimated from the McGill University weather station 250 m south of the experiment

This included a UHF vertical sounder which gave both reflectivity profiles and wind speed. Note that for f142, f207, the nominal rain rates estimated from the scenes in Desaulniers-Soucy et al. (2001) were 8—10 mm/h.

Table 1: Reproduced from [*Lilley, et al.*, 2005], characteristics of the HYDROP triplets.

3.2 Empirical test of the mass and number density laws on HYDROP data:

Fig 1a shows the 3D isotropic (angle averaged) spectrum of the 19 stereophotographic drop reconstructions averaged over each of the five storms. Each storm had 2 - 7 "scenes" (from matched stereographic triplets) with 5,000 – 20,000 drops each taken over a 15-45 minute period (see table 1). The angle averaging was done so that a white noise appears flat. The low wavenumber reference line indicates the theoretical Corrsin-Obukhov $k^{-(5/3+2)}$ angle averaged spectrum (the usual spectrum is angle integrated; the angle averaging -dividing by $4\pi k^2$ - contributes the 2 in the exponent). It can be seen that the transition between passive scalar behaviour - where the drops are effectively prisoners of the turbulence and the high wavenumber regime, where the drops are totally chaotic (white noise) occurs at scales of roughly 20-30cm. Many more details on these data sets are available in [*Lilley, et al.*, 2005], note however that the mean interdrop distance is about 10cm, so that at the transition scale there will be typically 10-50 drops.
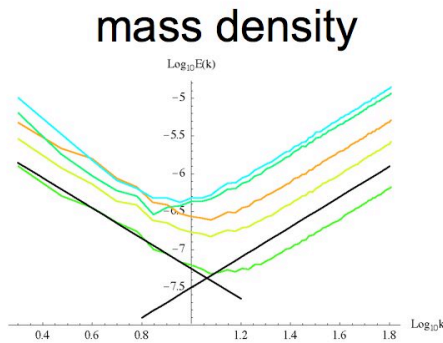

Fig. 1a: This shows the 3D isotropic (angle integrated) spectrum of the 19 stereophotographic drop reconstructions, for ρ, the particle mass density. Each of the five storms had 3- 7 "scenes" (from matched stereographic triplets) with 5,000 – 40,000 drops each taken over a 15-30 minute

period (orange = f207, yellow = f295, green = f229, blue green = f142, cyan = f145). The extreme low wavenumber corresponds to $\approx 2m$ ($\log_{10}k=0.3$, the minima correspond to about 20-40cm). The reference lines have slopes -5/3, +2, the theoretical values for the Corrsin-Obukhov ($l^{1/3}$) law and white noise respectively.

In order to test the $l^{1/2}$ law for the number density, we replaced each drop mass by the indicator function and produced the spectra shown in fig. 1b.
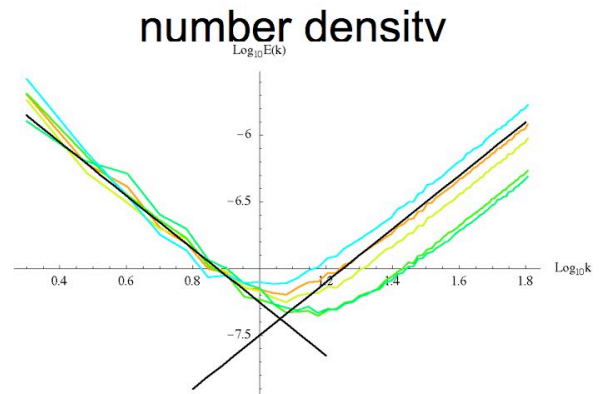

Fig. 1b: Same as previous but for *n*, the particle number density (calculated using an indicator function on a 128^3 grid. The reference lines have slopes -2, +2, the theoretical values for the $l^{1/2}$ law and white noise respectively.

In fig. 1b, we see that the convergence to the low wavenumber theoretical k^{-2} behaviour (straight line) occurs at slightly smaller scales than for the $k^{-5/3}$ behaviour of ρ since *n* is less variable (smoother) than ρ.

Finally, we display fig. 1c which show the ratio of the ensemble spectra (all 19 triplets) for $E_\rho(k)$, $E_n(k)$; this is a sensitive indication that the number density field really is smoother (by about $k^{1/3}$) than the corresponding spectrum for the mass density. Because we have taken the ratio of the spectra, the *y* axis is "blown up" with respect to the previous; this is quite a sensitive indicator that the basic theory is roughly correct.
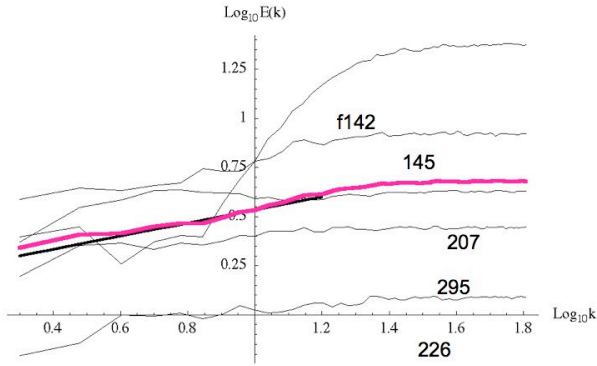
Fig. 1c: This shows the ratio of the ensemble spectra $E_\rho(k)/E_n(k)$; for each of the 5 storms, and the overall ensemble (purple), with theoretical reference line slope -1/3. This is a sensitive test of the prediction of eqs. 9, 25.

4. The compound Poisson-rain-turbulence model

4.1 Discussion

The general approach to numerical modelling of rain and clouds is to explicitly model the fluid dynamics and to parametrize the "cloud physics" i.e. the complicated coalesence, condensation and other particle scale processes are dealt with in a relatively ad hoc way. On the contrary, most attempts to explicitly deal with drop physics processes have made great simplifications in the fluid dynamics, usually ignoring the advection and turbulence (e.g. [*Srivastava and Passarelli*, 1980]), or occasionally by the converse: by including turbulence as a kind of parametrization of the coalescence kernel H; [*Khain and Pinsky*, 1995]. Other approaches which attempt both detailed microphysics and fluid dynamics (e.g. LES models, [*Khairoutdinav and Kogan*, 1999], actually end up parametrizing both the particle distributions (e.g. lognormal) and the small scale advection (see however [*Feingold, et al.*, 1998] for an LES with a "bin approach" to

the particle distribution). In all cases, the turbulent structures in the wind field are parameterized at scales much larger than the particle scales so that the kind of turbulent-drop interactions predicted by the number drop scaling law (eq. 25) coupled with the Corrsin-Obukhov law (eq. 9) are absent. Surprisingly, in the literature, we have found no reference to the Corrsin-Obukhov law in the context of rain drop-turbulence modeling.

In this section, we exploit the fact that the above derived turbulent scaling laws:

$$v_l = \varepsilon_l^{1/3} l^{1/3}$$
$$\rho_l = \chi_l^{1/2} \varepsilon_l^{-1/6} l^{1/3} \qquad (27)$$
$$n_l \approx A_l \chi_l^{1/2} l^{1/2}$$

to make a full explicit drop model valid from drop scales on up to the outer turbulent scales.

In terms of modelling particle behaviour, the modelling of *n* is critical since it can be used to control a Poisson process to determine particle positions. We can see from eq. 28 that it is jointly determined by the turbulent mass variance χ_l as well as by the drop processes via $A_l^{-2} = \left(\overline{M^2 v_R}\right)_l$ which we expect to vary only slowly as a function of scale *l*. We shall see that due to the scaling, eqs. 27 are actually very demanding on the way that water is distributed.

Before continuing, it is worth interpreting the key equation for n_l. We first note that since $1/n_l$ is the volume required so that there is typically a single particle, the local value of of n_l defines the (local) mean interparticle distance. Considering the number density at smallest scale of the turbulent cascade n_{l*} and averaging over the turbulence, we see that the typical interparticle distance is:

$$L_{int} \approx \left\langle n_{l_*} \right\rangle^{-1/3} = \frac{A^{-1/3}}{\left\langle \chi_{l_*}^{1/2} \right\rangle^{1/3} l_*^{1/6}} \qquad (28)$$

This equation shows how the mean interparticle distance is controlled by the large to small scale turbulent fluxes (χ), the inner scale of the cascade (l_*), and the drop

statistics/physics $\left(\overline{M^2 v_R}\right)$. In particular, for a given turbulent cascade process, $\left(\overline{M^2 v_R}\right)$ controls the typical interparticle distances.

4.2 Bare and dressed turbulent fields

Our aim is to produce a stochastic model which combines the turbulent cascade processes (to produce v_{l*}, ρ_{l*}, n_{l*}), with a small scale Poisson model of the drop processes. There are therefore two independent stochastic processes; the first determines the turbulent fields down to the smallest scale l_*, while the second, takes the first as given and distributes the drops and masses in such a way that at large enough scales, the degraded, averaged, "dressed" statistics follow at least roughly the observed Corrsin-Obukhov and corresponding number density laws.

The model starts by using a turbulent cascade to obtain stochastic realizations for the fluxes with the prescribed scalings (i.e. which obey eq. 27 for all scales $l \geq l_*$), and multifractal intermittencies i.e. the fluxes at scale l have the following multiscaling properties: $\langle \varepsilon_l^q \rangle = l^{-K_\varepsilon(q)}$; $\langle \chi_l^q \rangle = l^{-K_\chi(q)}$ where the K's are convex functions of the order of statistical moment q. In order to understand the model, we start with the distinction between bare and dressed cascade quantities (c.f. [*Schertzer and Lovejoy*, 1987]). The bare quantities are purely the result of turbulent cascade processes starting from a large external scale down to the smaller scale l, and stopped at that scale. In contrast, the "dressed" quantities (denoted with a subscript "d" below) are the result of continuing the cascade down to its smallest inner scale, denoted l_* (in principle the limit $l_* \to 0$ could be taken) and then spatially averaging over the corresponding scale l:

$$n_{d,l} = \frac{1}{volB_l} \int_{B_l} n_{l_*} d\underline{x}$$

$$\rho_{d,l} = \frac{1}{volB_l} \int_{B_l} \rho_{l_*} d\underline{x} \qquad (29)$$

Note that here and below, we drop explicit reference to time, but all of the results extend readily from space to space – time, as long as an appropriate space-time stratification is used and the causality of the resulting process is respected (see e.g. [*Marsan, et al.*, 1996]).

The relation between the bare and dressed quantities are relatively well understood. For example for the flux χ, we have $\chi_{d,l} = \chi_{h,(l//l_*)} \chi_l$ where $\chi_{h,(l//l_*)}$ is a "hidden" factor (hidden by the spatial integration [*Schertzer and Lovejoy*, 1987]), which is a random factor which most of the time is of order unity, but occasionally takes large values such that the tail of its probability distribution is algebraic with exponent q_D. This implies:

$$\langle \chi_l^q \rangle = l^{-K_\chi(q)}; \quad q \geq 0$$

$$\langle \chi_{l,d}^q \rangle \propto \begin{array}{ll} l^{-K_\chi(q)} & q < q_D \\ \infty & q \geq q_D \end{array} \qquad (30)$$

(strictly speaking the above divergence occurs in the limit $l_* \to 0$).

4.3 The Poisson drop field:

At the finest resolution l_*, the Poisson number density field $n_{p,l_*}(\underline{x})$ and the Poisson mass density field $\rho_{p,l_*}(\underline{x})$ (the "p" for "Poisson") can be defined as the random "Dirac comb":

$$n_{p,l_*,\infty}(\underline{x}) = \sum_i \delta(\underline{x} - \underline{x}_i) \qquad (31)$$

where the positions $\underline{x}_i$ are subordinated to the bare number density at the highest resolution n_{l*} and the sums are over all the particles indexed by I, and "δ" is the Dirac delta function. The second index l_* refers to the

resolution of the subordinating cascade process, the third index, to the scale of the Poisson drop process; in eq. 32 the symbol "∞" is used because the Dirac δ function has infinitely small resolution. This means that with the help of $n_{l_*}(\underline{x})$ we introduce the random Poisson measure $d\mu$ with the property that for any function $n_{l_*}(\underline{x})$ any set B_l:

$$Num\left(B_l\right) = \int_{B_l} n_{l_*}\left(\underline{x}\right) d\mu \tag{32}$$

where "$Num(B_l)$" means number of events in the set B_l. This is a Poisson random variable with the probability density:

$$\Pr\left(Num\left(B_l\right) = \nu\right) = \frac{\left(vol\left(B_l\right)n_{d,l}\right)^{\nu}}{\nu!} e^{-\left(vol\left(B_l\right)n_{d,l}\right)} \tag{33}$$

and the property:

$$\overline{\int_{B_l} n_{p,l_*,\infty}\left(\underline{x}\right) d\underline{x}} = vol\left(B_l\right)n_{d,l}$$

$$vol\left(B_l\right)n_{d,l} = \int_{B_l} n_{l_*}\left(\underline{x}\right) d\underline{x} \tag{34}$$

The overbar (here and throughout) indicates averaging with respect to the Poisson (drop) but not turbulent statistics.

Now that we have used the bare turbulent number density field n_{l*} to define a compound Poisson process for the drop locations, we must attribute a mass to each drop in such a way that the dressed Poisson density statistics will follow the Corrsin-Obukov law at large scales. To do this, we first define the corresponding Dirac comb for the masss density:

$$\rho_{p,l_*}\left(\underline{x}\right) = \sum_i M_i \delta\left(\underline{x} - \underline{x}_i\right) \tag{35}$$

Where the particle masses M_i must now be determined. To do this, we note that at the smallest turbulent scale l_*, we have a single drop so that the drop mass averaged over the Poisson process $\overline{M_i}$ is:

$$\overline{M_i} = \frac{\rho_{l_*}\left(\underline{x}_i\right)}{n_{l_*}\left(\underline{x}_i\right)} \tag{36}$$

The masses of each drop M_i may thus be chosen as:

$$M_i = u_i \frac{\rho_{l_*}\left(\underline{x}_i\right)}{n_{l_*}\left(\underline{x}_i\right)}; \quad \bar{u} = 1 \tag{37}$$

where the random variable u_i is taken from the unit dimensionless bare drop mass probability density $D(u)$.

The resulting Poisson process defines the (dressed) Poisson number and water densities as:

$$n_{p,l_*,l} = \frac{1}{vol\left(B_l\right)} \int_{B_l} n_{p,l_*,\infty}\left(\underline{x}\right) d\underline{x} \tag{38}$$

$$\rho_{p,l_*,l} = \frac{1}{vol\left(B_l\right)} \int_{B_l} \rho_{p,l_*,\infty}\left(\underline{x}\right) d\underline{x}$$

$$= \frac{1}{vol\left(B_l\right)} \sum_{\underline{x}_i \in B_l} M_i$$

We show in the next subsection that with this choice, for large enough l, the Poisson density field $\rho_{p,l_*,l}$ does indeed satisify the Corrsin-Obukhov law.

4.4 The dressed drop averaged statistics

Comparing eq. 34 with 38 we see that:

$$\overline{n_{p,l_*,l}} = n_{d,l}; \quad l > l_* \tag{39}$$

Since for larger and larger l, the Poisson averaging is over more and more particles, this actually implies:

$$n_{p,l_*,l} \approx n_{d,l} \approx n_l; \quad l >> l_*; \quad q < q_D \tag{40}$$

so that the Poisson number density field will follow the observed $l^{1/2}$ scaling law.

We now seek to determine some of the statistical properties of $\rho_{p,l_*,l}$, in particular to determine the conditions under which the mean for large enough l satisfies the Corrsin-Obukhov scaling law.

For the moment, we consider that the turbulent fields are fixed and seek the dressed statistics that result purely from the Poisson variability. To do this, we introduce the (Laplace) characteristic function $\Psi_{l,n}\left(q\right)$:

$$\Psi_{l,n}(q) = \overline{e^{q\nu}} = \sum_{\nu=0}^{\infty} \frac{\left(vol\left(B_l\right)n_{d,l}\right)^{\nu}}{\nu!} e^{-\left(vol\left(B_l\right)n_{d,l}\right)} e^{q\nu}$$
$$= e^{\left(vol\left(B_l\right)n_{d,l}\right)\left(e^q-1\right)}$$

(41)

Hence, the second characteristic function $K_{l,n}(q)$ is:

$$K_{l,n}(q) = \log \Psi_{l,n}(q) = \left(vol\left(B_l\right)n_{d,l}\right)\left(e^q - 1\right)$$

(42)

these are standard results for compound Poisson processes, see e.g. [*Feller*, 1971]. We can use this to calculate various statistics of $n_{p,l_*,l}$, for example, we can confirm eq. 40:

$$\overline{n_{p,l_*,l}} = \left.\frac{\partial e^{K_{n,l}(q)}}{\partial q}\right|_{q=0} = K'_{n,l}(0)$$

(43)

$$= \frac{1}{vol\left(B_l\right)} \int_{B_l} n_{l_*}(\underline{x}) d\underline{x} = n_{d,l}$$

We can now calculate the liquid water (ρ) statistics. First, define Ψ_u as the characteristic function of the random variable u with respect to D, we have:

$$\Psi_M(q) = \overline{e^{qM}} = \overline{e^{qu_i \rho_{l_*}(\underline{x})/n_{l_*}(\underline{x})}} = \Psi_u\left(q_i \frac{\rho_{l_*}(\underline{x})}{n_{l_*}(\underline{x})}\right)$$

(44)

where Ψ_M is the characteristic function with respect to the random variable M. We now use the additivity of K to integrate and obtain the second characteristic function of the total water in the set B_l (=$vol(B_l)\rho_{d,l}$):

$$K_{\rho,l}(q) = \int_{B_l} n_{l_*}(\underline{x}) \left[\Psi_u\left(\frac{q}{vol\left(B_l\right)} \frac{\rho_{l_*}(\underline{x})}{n_{l_*}(\underline{x})}\right) - 1\right] d\underline{x}$$

(45)

Applying this to calculate the Poisson averaged dressed density $\overline{\rho_{p,l_*,l}}$:

$$\overline{\rho_{p,l_*,l}} = \left.\frac{\partial e^{K_{\rho,l}(q)}}{\partial q}\right|_{q=0} = K'_{\rho,l}(0)$$

$$= \frac{1}{vol\left(B_l\right)} \int_{B_l} \Psi'_u(0) n_{l_*}(\underline{x}) \left[\frac{\rho_{l_*}(\underline{x})}{n_{l_*}(\underline{x})}\right] d\underline{x}$$

(46)

$$= \frac{1}{vol\left(B_l\right)} \int_{B_l} \rho_{l_*}(\underline{x}) d\underline{x} = \rho_{d,l}$$

where we have used the result for the exponential characteristic function: $\Psi_u(q) = 1/(1-q)$; hence $\Psi'_u(0) = \overline{u} = 1$. Note that the averaging is over the Poisson randomness, not the turbulence; and the above result establishes that the Poisson process when spatially averaged over large enough scales will follow the dressed turbulent (Corrsin-Obukhov) law.

Although this establishes that the mean ρ field will satisfy the Corrsin-Obukov scaling, this gives little information about the statistical fluctuations which we anticipate will be large; indeed, we expect the variability of the compound turbulent- Poisson process should be larger than for the original turbulent cascade process due to the "extra" Poisson variability. To study the variability, it is convenient to consider the moments higher than order 1 (the mean). For example, we can calculate the variance:

$$\sigma^2\left(\rho_{p,l_*,l}\right) = \overline{\rho_{p,l_*,l}^2} - \overline{\rho_{p,l_*,l}}^2$$

$$= \left.\frac{\partial^2 e^{K_{\rho,l}(q)}}{\partial q^2}\right|_{q=0} - \left(\left.\frac{\partial e^{K_{\rho,l}(q)}}{\partial q}\right|_{q=0}\right)^2$$

$$= K''_{\rho,l}(0)$$

(47)

$$= \frac{1}{vol\left(B_l\right)^2} \int_{B_l} \Psi''_u(0) n_{l_*}(\underline{x}) \left(\frac{\rho_{l_*}^2(\underline{x})}{n_{l_*}(\underline{x})}\right)^2 d\underline{x}$$

$$= \frac{\overline{u^2}}{vol\left(B_l\right)^2} \int_{B_l} \frac{\rho_{l_*}^2(\underline{x})}{n_{l_*}(\underline{x})} d\underline{x}$$

where we have used $\Psi''_u(0) = \overline{u^2}$. Using the Schwartz inequality, we obtain:

$$\int_{B_l} \frac{\rho_l^2}{n_l} d\underline{x} \int_{B_l} n_l \, d\underline{x} \geq \left(\int_{B_l} \rho_l \, d\underline{x}\right)^2$$

(48)

or:

$$\frac{1}{vol\left(B_l\right)^2} \int_{B_l} \frac{\rho_{l_*}^2}{n_{l_*}} d\underline{x} \geq \frac{\rho_{d,l}^2}{\int_{B_l} n_{l_*} d\underline{x}}$$

(49)

This, combined with $\overline{\rho_{p,l_*,l}} = \rho_{d,l}$ (eq. 46) implies:

$$\overline{\rho_{p,l_*,l}}^2 \geq \rho_{d,l}^2 \left(1 + \frac{\overline{u^2}}{\int\limits_{B_l} n_{l_*}(\underline{x}) d\underline{x}} \right) \qquad (50)$$

Note that for bare exponential unit drop size distributions $D(u)$ we have $\Psi_u''(0) = \overline{u^2} = 2$. The corresponding formula for the number density is:

$$\overline{n_{p,l_*,l}}^2 = n_{d,l}^2 \left(1 + \frac{1}{\int\limits_{B_l} n_{l_*}(\underline{x}) d\underline{x}} \right) \qquad (51)$$

This shows that the effect of the Poisson variability on the dressed variance is primarily in regions where the number density is low. Indeed, there are two different statistical ranges depending on whether $\int\limits_{B_l} n_{l_*}(\underline{x}) d\underline{x} \gg 1$ or $\ll 1$ (assuming that the bare unit drop size variance $\overline{u^2} \approx O(1)$). In the former, the effect of the Poisson randomness is negligible (hence we obtain the low wavenumber Corrsin – Obukhov statistics while in the latter, (high wavenumber regime), we obtain white noise statistics. To see this, recall that at small scales, $l < l_*$, $n_{l_*}(\underline{x})$ is smooth (roughly constant) so that for a ball $B_l(\underline{x})$ centred at point $\underline{x}$, we have:

$$\int\limits_{B_l(\underline{x})} n_{l_*}(\underline{x}') d\underline{x}' \approx l^3 n_{l_*}(\underline{x}) \qquad (52)$$

Also, noting that $n_{d,l_*} \approx n_{l_*}$ and using eq. 52, we obtain:

$$\overline{n_{p,l}}^2 \approx n_l l^{-3} \qquad (53)$$

For this small scale l^{-3} regime, we can find the corresponding spectrum using Parseval's theorem:

$$\overline{n_{p,l}}^2 \approx \int\limits_{1/l}^{\infty} E(k) dk \qquad (54)$$

($E(k)$ is the standard isotropic spectrum) we thus obtain (at large k) the white noise spectrum:

$$E(k) \approx k^2 \qquad (55)$$

4.5 The divergence of the third order moment of liquid water density

The various derivatives of K give the cumulants of various orders, and their relations with the moments of ρ become more and more complex for higher and higher orders. It is thus of interest to consider the "dressed η powers" defined by:

$$\rho_{p,l}^{(\eta)} = \frac{1}{vol(B_l)} \sum_{j \in B_l} M_j^\eta \qquad (56)$$

For example, for $\eta=2$, this corresponds to the radar reflectivity factor: $\rho_{p,l}^{(2)} = Z_l$; other values of η correspond to number density ($\eta=0$), the liquid water content ($\eta=1$) and the nominal rain rate ($\eta =7/6$; assuming the nominal fall speed is proportional to the drop radius).

The corresponding second characteristic function is:

$$K_{\rho,\eta,l}(q) = \int\limits_{B_l} n_{l_*}(\underline{x}) \left(\Psi_u \left(\frac{q}{vol(B_l)} \left(\frac{\rho_{l_*}(\underline{x})}{n_{l_*}(\underline{x})} \right)^\eta \right) - 1 \right) d\underline{x}$$

$$(57)$$

Hence:

$$\overline{\rho_{p,l}^{(\eta)}} = K'_{\rho,\eta,l}(0) = \frac{1}{vol(B_l)} \int\limits_{B_l} n_{l_*} \left(\frac{\rho_{l_*}}{n_{l_*}} \right)^\eta d\underline{x}$$

$$= \frac{1}{vol(B_l)} \int\limits_{B_l} \left(\overline{M^2 v_R} \right)_{l_*}^{(\eta-1)/2} \chi_{l_*}^{1/2} \varepsilon_{l_*}^{-\eta/6} l_*^{(3-\eta)/6} d\underline{x}$$

$$(58)$$

The key here is the exponent of the l_* factor. This shows that for $\eta>3$, in the limit $l_* \to 0$,

$$\overline{\rho_{p,l}^{(\eta)}} \to \infty; \quad \eta > 3 \qquad (59)$$

This implies that:

$$\Pr\left(\rho_{p,l}^{(\eta)} > s\right) \approx s^{-q_D}; \quad q_D = 3; \quad s >> 1 \quad (60)$$

We have already mentionned that cascade processes generally display divergence of high order statistical moments (eq. 59, 60 assumes that this q_D associated with the statistics of χ, ε, is >3; otherwise it will dominate that introduced by the Poisson process); eq. 58 shows that compound Poisson process have greater variability than the subordinating cascade process provides a totally new mechanism for the divergence. Fig. 2a shows that this prediction of divergence of moments $q=3$ and higher is well verified numerically on simulations (this simply checks that the above formulae are properly derived), and fig. 2b shows that the prediction is reasonably verified on the HYDROP data (see the next section), and figs. 2c, d show some rain rate probabilities that also display $q_D \approx 3$. An early review of the q_D values for rain may be found in [*Lovejoy and Schertzer*, 1995].
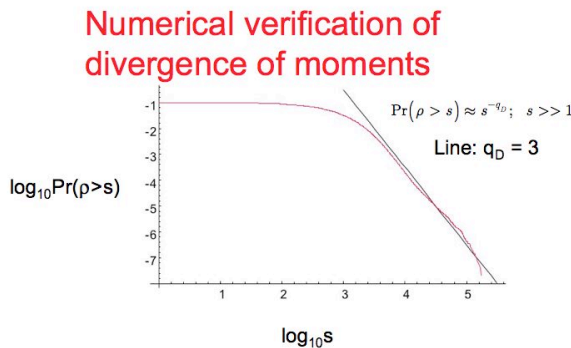
Lines: $\quad \Pr(\rho_{p,l} > s) \approx \left(\dfrac{s}{s_l}\right)^{-q_D}; \quad s_l = s_1 l^H; \quad H = -0.6 \quad q_D = 3$

Fig. 2b: The 19 HYDROP triplets are analyzed by calculating the total liquid water mass in cubes of size l as indicated. The graph shows the log probability of the liquid water exceeding a threshold $s=M_{p,l}$ for various scales. The thin lines are from the data analysis, the thick dashed lines are the results of the multifractal-compound Poisson model described in the text. The straight lines have the theoretical slope -3.

Fig. 2a: The probability distribution estimated from 20 independent realizations of the compound-multifractal Poisson process (with same parameters as in fig. 3 in next section). The theoretical prediction of eq. 59 is extremely well verified by the numerics.
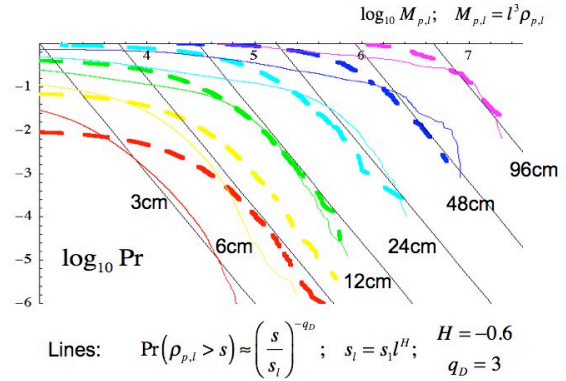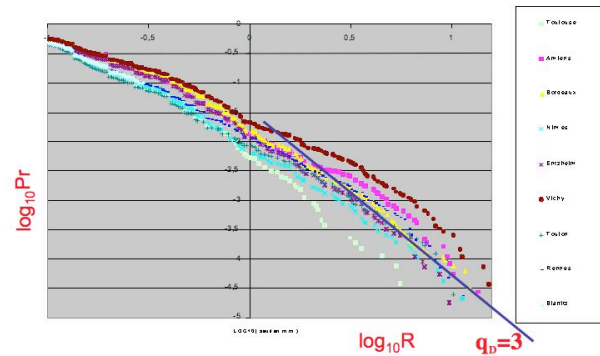

Fig. 2c: Rain rate data at 3minute resolution from 9 different French stations on a log log plot (lowest probability indicated in 10^{-5}). The reference line with slope $q_D=3$ is shown indicating that the rain rate has extremes not far from that predicted for the liquid water content. (From Y. Tchigirinskaya, personal communication).
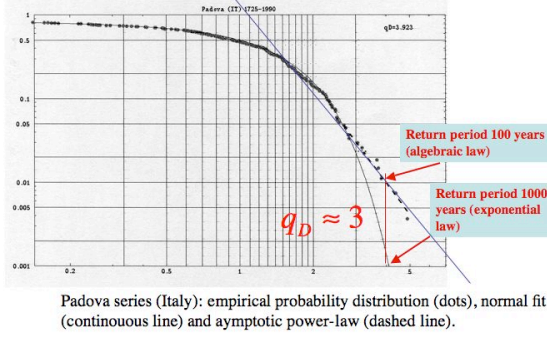
Fig. 2d: Daily rain rate probability distribution from one of the longest available series (Padova, Italy). predicted q_D=3 behaviour is shown for reference and fits the data very well. Reproduced from [*Bendjoudi*, 1997].

5. Numerical implementation of the model

5.1 The turbulent cascade:

The first step in the numerical simulation is to simulate the bare multifractal cascade quantities n, ρ. This requires the two fluxes ε, χ; as mentioned above, these fluxes are presumably correlated. A convenient but by no means unique way to account for this is to take:

$$\chi = \phi^{2/3}\varepsilon^{1/3} \tag{61}$$

where ϕ, ε are independent multifractal cascades; this equation implies correlations between χ and; it yields:

$$\begin{aligned} \rho_l &= \phi_l^{1/3}l^{1/3} \\ n_l &= A_l\phi_l^{1/3}\varepsilon_l^{1/6}l^{1/2} \end{aligned} \tag{62}$$

(15)

where A_l is a (dimensional) constant which determines the mean interdrop distance (c.f. eqs. 25). The advantage of the choice 61 is that no (possibly divergent) negative moments of turbulent fluxes needed to determine n, ρ. In order to simulate cascades with the statistics eq. 27, we use the Fractionally Integrated Flux (FIF) model ([*Schertzer and Lovejoy*, 1987], [*Schertzer, et al.*, 1997]) which essentially interprets the linear scaling factors $l^{1/3}$, $l^{1/2}$ as fractional integrals of order 1/3, ½. This is performed with convolutions between the multifractal fluxes ϕ, ε and singularities. For simplicity, we choose ϕ, ε to be identical, independent multifractal process. In addition, we use the two-parameter universal multifractal processes (with Levy generators) with the following statistics:

$$\left\langle \varepsilon_l^q \right\rangle = \left\langle \phi_l^q \right\rangle = l^{-K(q)}$$

$$K(q) = \frac{C_1}{\alpha - 1}\left(q^\alpha - q\right) \tag{63}$$

Where $0 \le C_1 < d$, is the codimension of the mean and characterizes the sparseness of the mean process (d is the dimension of the embedding space, d=1 in fig. 3b, d=3 in fig. 5a, b), and $0 \le \alpha \le 2$ is the Levy index characterizing the degree of mulitfractality (0 is the monofractal minimum, α=2 is the "log-normal" maximum). More details may be found in the above cited references, see fig. 3a, b for examples in 1-D.
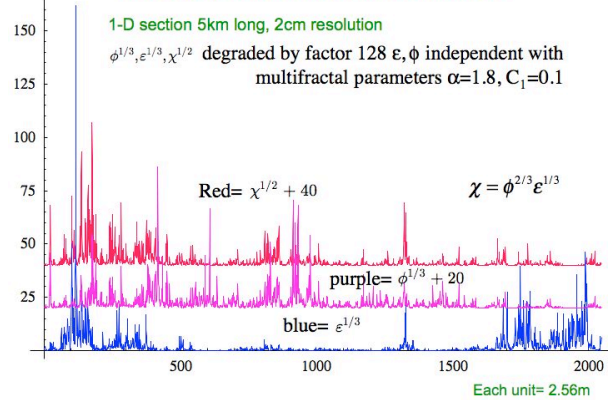

Fig. 3a: This figure shows the three turbulent fluxes (ε, χ, ϕ), offset in the vertical for clarity. The ϕ, ε fluxes are statistically independent realizations of a universal multifractal processes characterized by C_1=0.1, α=1.8 (close to those estimated for HYDROP, see [*Lilley, et al.*, 2005]). This is already a low resolution (degraded by a fctor of 128) version of the full simulation which had resolution of 2cm over a total distance of 5km.
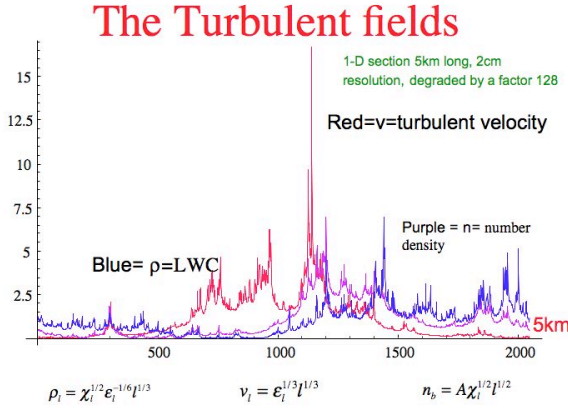
Fig. 3b: This shows the turbulent fields derived by fractional integration from the fluxes in fig. 3a.

Once the ρ, $\phi_l^{1/3}\varepsilon_l^{1/6}l^{1/2}$ fields have been calculated down to scale l_*, the value of the normalization constant A of n is chosen so that the desired mean interparticle distance is obtained. To be meaningful, we must choose A such that $L_{int}>l_*$ i.e. so that there are generally fewer drops than grid points/boxes. This is necessary since with a gridded model there cannot meaningfully be more than one particle per grid box, hence we simulate in a regime where the probability of more than one particle being in a grid box is low. We then attribute the particles to the grid boxes with a Poisson process controlled by n. The masses are then attributed to each particle by using a unit exponential distribution for $D(u)$ (c.f. eq. 37) so that at the bare level, the drop size distribution is the Marshall-Palmer (exponential) with amplitude given by the ratio ρ/n.

5.2 Results of the simulation

Fig. 4 shows results of the numerical implementation of the process. The constant A was chosen so that the spatial mean of the number density for the realization of n=0.1, with 1 grid box =2cm (so as to be close to the HYDROP results). The turbulent cascades were produced using the universal multifractal

model ([*Schertzer and Lovejoy*, 1987], [*Schertzer, et al.*, 1997], [*Schertzer and Lovejoy*, 1997]) with using typical measured turbulent parameters.
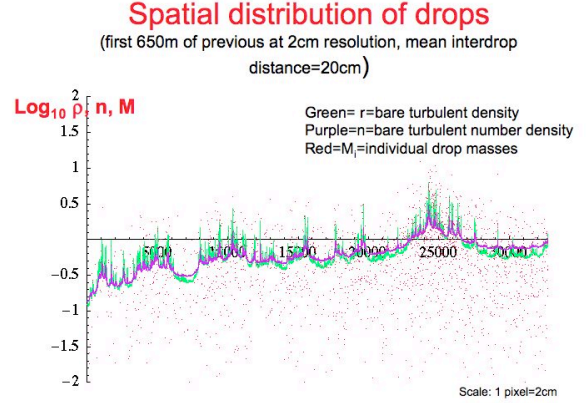

Fig. 4a: This figure shows the full (2cm) resolution of the 1-D simulation in fig. 3b with the dots indicating the positions and masses (on log scale) of the drops. The green field is the bare turbulent mass density, the purple is the bare number density.
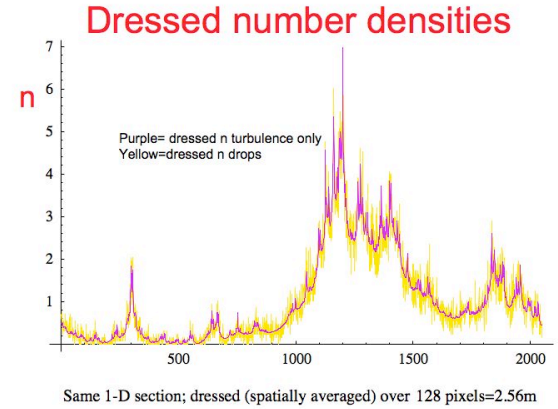

Fig. 4b: This figure shows the dressed (degraded by factor 128) 2.56m resolution comparison of number density fields: $n_{d,l}$, $n_{p,l}$ with l=2.56m. As expected the two are the same except for high frequency noise due to the Poisson process.

Dressed LWC densities

Blue= dressed ρ turbulence only
Green=dressed ρ drops

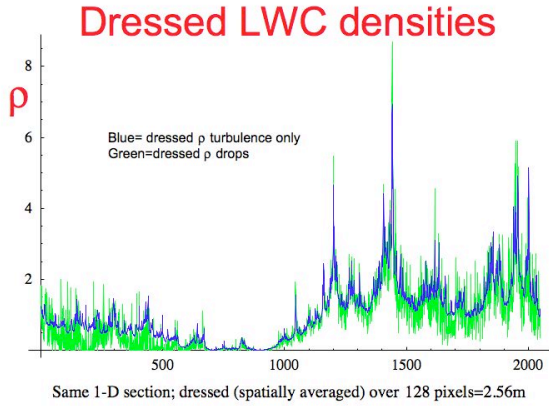Same 1-D section; dressed (spatially averaged) over 128 pixels=2.56m

Fig. 4c: This figure shows the dressed (degraded by factor 128) 2.56m resolution comparison of mass density fields: $\rho_{d,l}$, $\rho_{p,l}$ with l=2.56m. As expected the two are the same except for high frequency noise due to the Poisson process.

In fig. 5a, we show a cross-section through a corresponding 3D model (also with 2cm resolution with 128^3 pixels so that the result is quite close to the observed HYDROP domain size. In fig. 5b, we show a perspective plot comparing the simulation and the one of the HYDROP reconstructed 3D distributions.

3D Multifractal-Turbulence Poisson-Drop model

2m   (Isotropic)

In the following, 1 pixel=2cm, model=128x128X128cm, 20,000 drops (mean interdrop distance=10cm)

v=Turbulent velocity

n=Number density

ρ=LWC density

False colour of the bottom number density field
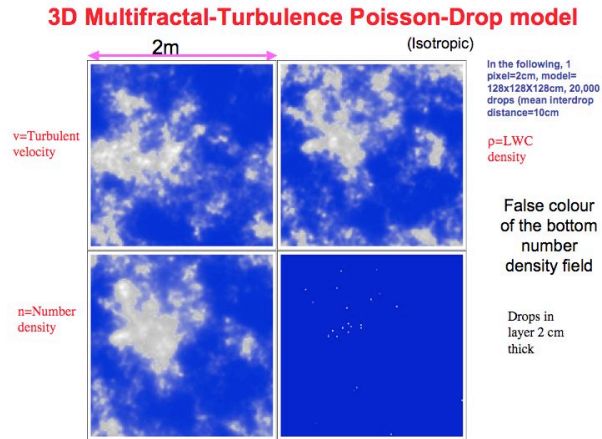
Drops in layer 2 cm thick

Fig. 5a: 2D cross-sections through a 3D model (same parameters as the 1D model in fig. 4, also with 2cm resolution) with 128^3 pixels so that the result is quite close to the observed HYDROP domain size.
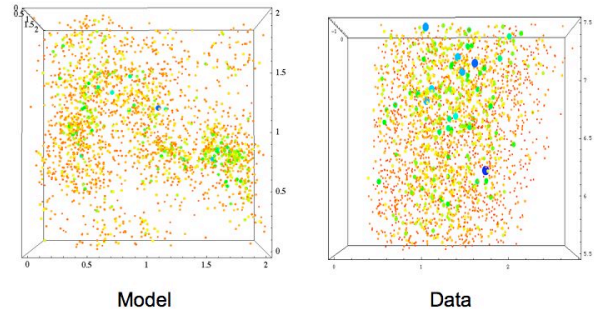
Model data intercomparison

Model   Data

Fig. 5b: The simulation is the full 3D simulation from fig. 5a. The data is from HYDROP triplet (day 295, 2nd triplet). The drop diameters are proportional to the true diameters, the colours also are size determined.

The density: anisotropic extensions:
examples varying the anisotropy

(Visualized using single scattered visible radiation, using the threshold approximation, 30% above threshold, 3D, with vedrtical stratification…)
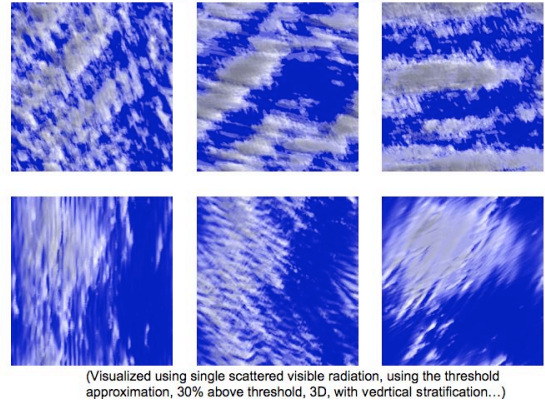
Fig. 5c: These show simulations at much larger scales using the threshold approximation (see text), with simulated radiative transfer (single scattering only, isotropic phase functions). The basic fields here are 3D with stratification in the vertical according to lidar measured stratification exponents ([*Lilley, et al.*, 2004]).

5.3 Some statistical properties of the compound Poisson-Multifractal process:

We have already theoretically derived some of the statistical properties of the model. A fuller understanding of model the will be the subject of future work. However, the low *n* behaviour is important in verifying the model

against the HYDROP data, especially the transition near the mean interdrop scales. We therefore display fig. 6 which shows that both the liquid water density and number densities do indeed follow the theoretical turbulent field behaviours at low wavenumbers, but at high wavenumbers undergo a transition to white noise behaviour (quite close to the HYDROP behaviour, see fig. 6, see eq. 56).
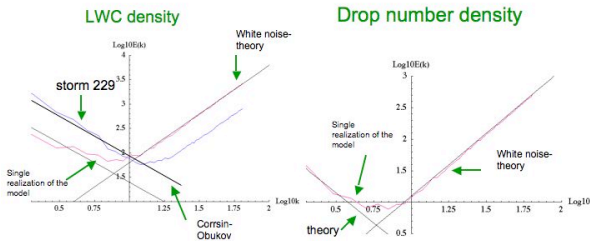

Fig. 6: These show the 3D spectra of the HYDROP LWC data and simulation (left), and simulation number density (right), the model using the simulation shown in fig. 5. The low and high frequency behaviour is as described by the theory lines, see text.
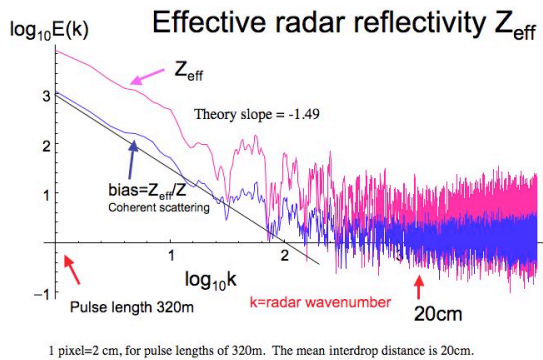

Fig. 7: This shows how the model can be used to study issues of radar calibration; here we show the effect of coherent scattering can bias the estimates of Z from the measured Z_{eff}. The red is the raw Z_{eff} the blue is the same but normalized by the corresponding Z (i.e. it is the bias). This 1D simulates a rain field with 2cm resolution, with

mean interdrop distance 20cm, and pulse length 320m. The bias (Z_{eff}/Z) due to the coherency effects (blue) is negligible until wavelengths of 50-60cm are reached, and can become very large for long wavelengths.

6. Conclusions:

On the basis of both turbulence, drop coalesence theory and state-of-the-art drop size/position stereophotographic data, we have argued that the rain liquid water density at large enough scales follows Corrsin-Obukhov passive scalar statistics ($k^{-5/3}$ spectrum) and that also at low wavenumbers, the particle number density they follows a new k^{-2} law which we derive by combining turbulence and drop coalesence theory. At smaller scales, due to the decoupling of the wind and the drops, we observe white noise k^{+2} spectra (in 3D). The key point is that since coalescence processes conserve mass, but not number density, the ρ statistics are entirely due to the concentration of mass from large scale to small via turbulent cascade processes. However, for the number density, the situation is different because both the large and small (drop) scale processes determine the number density. This allows for the different scaling laws (in real space $l^{1/3}$ for ρ, $l^{1/2}$ for n).

We can use the turbulent number density (n) field, to subordinate a compound multifractal-Poisson process whose mean (over the Poisson but not turbulent statistics) is the turbulent number density. In addition, if we use both ρ and n, then we can attribute masses to the Poisson distributed particles in such a way as to recover the large scale LWC statistics; we show how this may be done using a marginal exponential (Marshall-Palmer) distribution for the drops. Although the drop size distribution is thin-tailed (here we used an exponential "Marshall-Palmer" type) as concerns the distribution of liquid water within a region size l, the generic result

is a "fat-tailed" algebraic distribution. We showed this theoretically, numerically and also empirically on the HYDROP data, indicating that this could be the explanation of several empirical observations of q_D=3 rainrate statistics. We did not discuss the considerably more involved issue of drop size distributions. However, it is clear that the latter will be a systematic function of resolution, and this in itself will already help explain the apparent lack of "universality" of empirical drop-size distributions.

An important limitation of the model presented in this paper we do not calculate rain rate statistics. While this is easy enough to do by attributing a nonturbulent velocity to each drop, there is no unique way to assign the velocities and the extension of the model will thus be the subject of future work.

One of the main applications of the model will be to study issues of rainfall measurement from either rain gages, or radar. In fig. 7 we give an example of how the model can be used to calculate both the radar reflectivity factor (Z) and the effective reflectivity factor Z_{eff} (which is what the radar actually measures, it takes into account the wave coherency effects). More applications of this sort will be discussed in future publications.

Finally, we indicated briefly how the model can be used at very large scales for cloud and radiative transfer calculations. The key is to make an approximation for the low n part of the process; here only the simplest (threshold) approximation was used. More sophisticated treatment of the low n properties of the model may help answer basic questions about low rain rate, low radar reflectivity statistics, measurements.

6. References

Anselmet, F., R. A. Antonia, L. Danaila (2001), Turbulent flows and intermittency in laboratory experiments, *Plan. and Space Sci.*, *49*, 1177-1191.

Bendjoudi, H., Hubert, P., Schertzer, D., Lovejoy, S. (1997), Interprétation multifractale des courbes intensité-durée-fréquence des précipitations, Multifractal point of view on rainfall intensity-duration-frequency curves, *C.R. A. S., (Sciences de la terre et des planetes/Earth and Planetary Sciences)*, *325*, 323-326.

Desaulniers-Soucy., N., et al. (2001), The continuum limit in rain and the HYDROP experiment, *Atmos. Resear.*, *59-60*, 163-197.

Falkovitch, G., and A. Pumir (2004), Intermittent distribution of heavy particles in a turbulent flow, *Phys. Fluids*, *16*, L47-L50.

Falkovitch, G., et al. (2006), Rain initiation time in turbuloent warm clouds, *J. Applied Meteorology and Climatology*, *45*, 591-599.

Feingold, G., et al. (1998), Simulations of marin stratocumuls using a new microphysical parametrization scheme, *Atmos. Res.*, *47-48*, 505-528.

Feller, W. (1971), *An Introduction to probability theory and its applications, vol. 2*, 669 pp., Wiley, New York.

Jameson, A. R., and A. B. Kostinski (1999), Fluctuation properties of precipitation: Part V: Distribution of rain rates – theory and observations in clustered rain, *J. Atmos. Sci.*, *56*, 3920–3932.

Khain, A. P., and M. B. Pinsky (1995), Drop Inertia and its contribution to trublent coalescence in coonvective clouds. Part I: Drop fall in the flow with random horizontal velocity, *J. Atmos. Sci.*, *52*, 196-206.

Khairoutdinav, M., and Y. Kogan (1999), A new cloud physics paramterization in a Large-Eddy Simulation model of marine stratocumulus, *Mon. Wea. Rev.*, *128*, 229-243.

Lilley, M., et al. (2005), Multifractal large number of drops limit in Rain, *J. Hydrol.*, *doi:10.1016/j.jhydrol.2005.11.063*,

Lilley, M., et al. (2004), 23/9 dimensional anisotropic scaling of passive admixtures using lidar aerosol data, *Phys. Rev. E*, *70*, 036307-036301-036307.

Lovejoy, S., et al. (2004), Bubble distributions and dynamics: the expansion-coalescence equation, *J. Geophys. Res. (Solid Earth)*, *109*, B, *doi:10.1029/2003JB002823.*, 11203.

Lovejoy, S., et al. (2003), Large particle number limit in Rain, *Phys. Rev. E*, *68*, 025301.

Lovejoy, S., and D. Schertzer (1990), Fractals, rain drops and resolution dependence of rain measurements, *Journal of Applied Meteorology*, *29*, 1167-1170.

Lovejoy, S., and D. Schertzer (1991), Multifractal analysis techniques and the rain and clouds fields from 10^{-3} to 10^{6}m, in *Non-linear variability in geophysics: Scaling and Fractals*, edited by D. Schertzer and S. Lovejoy, pp. 111-144, Kluwer.

Lovejoy, S., and D. Schertzer (1995), Multifractals and Rain, in *New Uncertainty Conceps in Hydrology and Water Ressources*, edited by Z. W. Kunzewicz, pp. 62-103, Cambridge University Press.

Marsan, D., et al. (1996), Causal space-time multifractal processes: predictability and forecasting of rain fields, *J. Geophy. Res.*, *31D*, 26,333-326,346.

Marshall, J. S., and W. Hitschfeld (1953), Interpretation of The fluctuating Echo from Random Distributed Scatterers; Part I., *Canadian Journal of Physics*, *31*, 962-994.

Schertzer, D., and S. Lovejoy (1987), Physical modeling and Analysis of Rain and Clouds by Anisotropic Scaling of Multiplicative Processes, *Journal of Geophysical Research*, *92*, 9693-9714.

Schertzer, D., and S. Lovejoy (1997), Universal Multifractals do Exist! *J. Appl. Meteor.*, *36*, 1296-1303.

Schertzer, D., et al. (1997), Multifractal cascade dynamics and turbulent intermittency, *Fractals*, *5*, 427-471.

Srivastava, R. C., and R. E. Passarelli (1980), Analytical solutions to simple models of condensation and coalescence, *J. Atmos. Sci.*, *37*, 612–621.

Uijlenhoet, R., et al. (1999), Towards a stochastic model of rainfall for radar hydrology: testing the Poisson homogeneity hypothesis, *Phys. Chem. Earth (B)*, *24*, 747–755.

Wallace, P. R. (1953), Interpretation of The fluctuating Echo from Random Distributed Scatterers; Part II, *Canadian Journal of Physics*, *31*, 994-1009.